Fermi National Accelerator Laboratory

FN-346
1500.000

NON-REPEATABILITY and CHAOTIC TRAJECTORIES in BEAM-BEAM INTERACTION SIMULATIONS at $p\bar{p}$ COLLIDER PARAMETERS

D. Neuffer, A. Riddiford and A. G. Ruggiero

Fermi National Accelerator Laboratory, Batavia, Illinois 60510

November 1981

Operated by Universities Research Association Inc. under contract with the United States Department of Energy

FN-346
1500.00

Non-Repeatability and Chaotic Trajectories in Beam-Beam Interaction Simulations at $p\bar{p}$ Collider Parameters

D. Neuffer, A. Riddiford and A.G. Ruggiero

October, 1981

ABSTRACT

Analyses of particle dynamics in a simulation of the 2-D "beam-beam" interaction shows evidence of non-repeatable, "chaotic" trajectories. A non-zero entropy for the transformation is deduced. This requires an asymmetric transformation ($\nu_x \neq \nu_y$) and large dynamic resonances to be significant. However, a round beam does not show large phase space blow-up, and any changes in rms emittances are associated with the "chaotic" trajectories.

I. Introduction

In proton-antiproton ($p\bar{p}$) collisions in the "Tevatron"[1], particle trajectories will be affected by the highly nonlinear force of the "beam-beam" interaction, that is, the electromagnetic force field of the opposite beam in the collisions. Recent theoretical, numerical and experimental investigations[2,3] have not placed precise limits on the effects of the force. It has been recognized that this case is an example of a nonlinear dynamic system, and these systems have recently been subjected to detailed studies.

In the present paper we approximate particle circulation around the ring as the product of two transformations: a linear transport around the storage ring followed by a nonlinear beam-beam "kick" at the interaction area.

Transport around the ring can be represented by a 2x2 matrix for both transverse (x and y) dimensions:

$$\begin{pmatrix} x \\ x' \end{pmatrix}_{\text{After}} = \begin{bmatrix} \cos 2\pi\nu_x & \beta_x \sin 2\pi\nu_x \\ \dfrac{\sin 2\pi\nu_x}{\beta_x} & \cos 2\pi\nu_x \end{bmatrix} \begin{pmatrix} x \\ x' \end{pmatrix}_{\text{Before}} \qquad (1)$$

In this linear transport x and y motion are decoupled. ν_x, ν_y, β_x, β_y are the usual Courant-Snyder tunes and beta-functions. The beam-beam kick can be represented as

$$\begin{pmatrix} x \\ x' \end{pmatrix}_{\text{After}} = \begin{bmatrix} 1 & 0 \\ -\dfrac{4\pi\Delta\nu_x}{\beta_x} F_x(x,y) & 1 \end{bmatrix} \begin{pmatrix} x \\ x' \end{pmatrix}_{\text{Before}} \qquad (2)$$

with a similar expression for y, y'.

The product of these transformations is equivalent to integration of the equation of motion:

$$x'' + K_x(s)\, x = -\frac{4\pi\Delta\nu_x}{\beta_x} F_x(x,y)\, x\, \delta_p(s) \qquad (3)$$

s, the distance along the storage ring, is the independent variable and $\delta_p(s)$ is a periodic delta-function.

In the present report we choose parameters which approximate the conditions[1] in the Tevatron: $\Delta\nu_x=\Delta\nu_y=0.01$, $\beta_x=\beta_y=2$ m and we choose

$$F_x = F_y = \frac{1 - e^{-(x^2+y^2)/2\sigma^2}}{(x^2+y^2)/2\sigma^2} \qquad (4)$$

with σ = 0.0816 mm which is the nonlinear force due to a round, gaussian charge distribution of rms radius σ. We compare three cases:

Case A: $\nu_x=\nu_y=.245$ on a 1/4,1/4 resonance

Case B: $\nu_x=.245$ $\nu_y=.12$ on a 1/4,1/8 resonance

Case C: $\nu_x=.3439$ $\nu_y=.1772$ "resonance-free"

We are investigating in detail the long time stability of these cases with the beam-beam interaction[4,5,6]. It has been suggested that such nonlinear systems may show instability properties undesirable in a $p\bar{p}$ collider, and our simulations are a search for such properties.

II. Repeatability Test Result

Simulation of millions of turns in particle trajectories requires extremely high accuracy. As a fundamental test of accuracy we have run repeatability tests for these trajectories. In these tests a particle trajectory is run forward for many turns following transformations (1) and (2), and is then returned by reversing these transformations. Forward and return positions are compared. As noted in reference 4, double precision accuracy is required, and produces agreement between initial and final positions to $\sim$15 significant figures after 120 million total turns for typical trajectories in cases A and C of references 4 and 5.

It is expected that each turn of calculation will introduce numerical error. If the errors are simply additive we find, for each phase space coordinate x,

$$x \to x_o + \sum_{i=1}^{N} \delta_i \tag{5}$$

after N turns where δ_i is the error at the turn i, and the sum is the accumulated error. The rms accumulated error is

$$\Delta \equiv \langle (x-x_o)^2 \rangle^{1/2} = \langle (\Sigma\, \delta_i)^2 \rangle^{1/2} = N^{1/2} \langle \delta^2 \rangle^{1/2} \tag{6}$$

The separate errors δ_i are uncorrelated and the resulting total error is $N^{1/2}\ \delta_o$, where δ_o is an rms error per turn. For our simulations $\delta_o \tilde{=} 10^{-26}$ and $N \tilde{=} 10^8$, so $\Delta \lesssim 10^{-22}$; this is not our major source of error.

A more important source of error is the tune error. An error δ_i in position leads to an error $\delta\nu_i$ in tune through the nonlinear beam-beam interaction and this leads to an accumulated error in phase of the order $(N-i)\ \delta\nu_i$. The accumulated error from such "phase slippage" is

$$\Delta = \langle (x-x_o)^2 \rangle^{1/2} = \left\langle \sum_{i=1}^{N} \left(R(N-i)\ \delta\nu_i\right)^2 \right\rangle^{1/2}$$

$$= \alpha\, N^{3/2}\, \delta_o \qquad (7)$$

Here α is some factor of order unity from the summing procedure. The $\delta\nu_i$ errors are assumed to be uncorrelated. R and ϕ are simply the amplitude and phase in $x=R\cos\phi$ (amplitude-phase variables) $(\phi \tilde{\nu} N + \phi_o)$ and we have ignored numerical factors of order unity in obtaining our final expression. This phase slippage leads to errors of order 10^{-14} for $\tilde{\delta}=10^{-26}$, $N=10^8$ and is the major source of accumulated errors in normal trajectories. In Figure 1 we display accumulated errors for several normal trajectories, where particles are transported 60 million turns forward and then returned. Forward and return positions are compared and results of these comparisons are shown.

In case B ($\nu_x=.245$, $\nu_y=.12$, $\Delta\nu=.01$), some particle trajectories show radically different behavior; they fail the repeatability test completely after only $\sim$100,000 turns. The other trajectories in the same case retain $\sim$14-16 decimal digit accuracy for 120 million turns. In a sample of 500 trajectories, selected randomly within a gaussian distribution in the 4-D phase space, 25% fail repeatability after $\sim$100,000 turns and 75% show $\gtrsim$20 digit accuracy consistent with 14 digit, 120M turn precision. We

tentatively label the nonrepeatable trajectories as "chaotic" trajectories.

In Figure 2 we display the accumulated error for a "chaotic" trajectory which quickly loses all correlation with its forward position after only 16,000 return turns. The straight line in the logarithmic error plot indicates errors accumulate exponentially. Empirically we find:

$$\delta x \simeq e^{+aN} \delta_o \tag{8}$$

where a is a constant which $\cong$ .001 and $\delta_o \tilde{=} 10^{-26}$. This type of error growth is what would occur in an unstable region in which a small deviation departs from an initial point exponentially.

Empirically we see very similar behavior in a single precision calculation, except that $\delta_o \tilde{=} 10^{-13}$. Table 1 and Figure 3 summarize some results of double precision and single precision tests of "chaotic" trajectories. Precision does not change the nature of the chaotic behavior. In Table 1 we display and compare the number of turns at which errors of 10^{-23}, 10^{-18}, 10^{-13} and 10^{-8} appear in double precision, and errors of 10^{-9} and 10^{-4} in single precision. The growth of errors remains exponential, as can be seen from Table 1 by noting

$$N(10^{-8})-N(10^{-13}) \cong N(10^{-13})-N(10^{-18}) \cong N(10^{-18})-N(10^{-23})$$

$$\text{and } N(10^{-8})-N(10^{-13})_{\text{double precision}} \cong$$

$$N(10^{-4})-N(10^{-9})_{\text{single precision}} \tag{9}$$

where N is the number of turns to reach a particular error level. This means that equation (8) accurately describes the error growth. Also, from

Table 1, it can be seen that the parameter in equation (8), "a", does not depend on precision but it does depend on particle trajectory. In mathematical terms, "a" is "partition-independent".

The next question we ask is whether these chaotic trajectories define a compact region in phase space. In Figure 4A we show the initial 4-D positions of chaotic trajectories projected onto x-x′ and y-y′ phase spaces as well as positions of normal trajectories. A clear boundary between types is not evident, although chaotic trajectories are clustered noticeably near the $\nu_x=1/4$ and $\nu_y=1/8$ resonances. In Figure 4B we show 127 initial coordinates for chaotic trajectories; the same clustering can be seen.

However, a projection along one dimension does show a clear boundary. If we choose initial $x'=y'=0$ and $x=y$, we find normal trajectories for $x_{initial}\leq .1101$ and $x_{initial}\geq .1395$. Chaotic trajectories are seen when $.1102\leq x_{initial}\leq .1394$. In figures 5A and 5B we compare 4 of these trajectories: A: $x_i=.1101$, B: $x_i=.1102$, C: $x_i=.1394$, D: $x_i=.1395$. After 30,000 turns forward and return trajectories B&C, which were originally extremely close to A&D, have clearly deviated, following $\nu_x=1/4$, $\nu_y=1/8$ separatices. The clear boundary in a 1-D projection is evidence for a separation of chaotic and normal regions, which is not evident in 2-D projections because of the complexity of 4-D phase space.

III. Non-repeatability and Entropy

Recent mathematical research associates loss of information in a transformation with "entropy"[7,8].

We begin by describing the entropy H associated with a particular partition $\{p_m\}$ of phase space, where $\{p_m\}$ is a finite set of subsets whose union is all space. We use

$$H = \sum_m \mu(p_m) \ln \mu(p_m)$$

where $\mu(p_m)$ is a measure function normed so that

$$\sum_m \mu(p_m) = 1$$

The mapping transforms the partition $\{p_m\}$ into a new partition $\{Tp_m\}$ which can be "joined" with $\{p_m\}$ to form a "least upper bound" partition $\{p_m\}V\{T\ p_m\}\equiv T^1 p_m$ which defines an "entropy"

$$H_1 = \Sigma\ \mu(T^1 p_m) \ln \mu(T^1 p_m)$$

where the sum is not over m but over all elements of the new partition. Successive mappings generate new partitions

$$T^n p_m = \{p_m\}\ V\ \{Tp_m\}\ V\ \{T^2 p_m\}....V\{T^n p_m\}$$

with entropies H_n. An "entropy per unit time" of T, p_m is defined by

$$h(p_m,T) = \lim_{n\to\infty} \frac{H_n}{n}$$

The "entropy of the transformation T" is the supremum of $h(p_m,T)$ over all finite partitions $\{p_m\}$:

$$h(T) = \sup_{p_m} h\,(p_m,T)$$

These entropies can be associated with an "information rate" of the transformations as can be demonstrated by a simple example.

For our example we choose a partition of the unit interval into tenths and choose a mapping of the unit interval into itself by T(x)=fractional part of (10x). Each transformation reveals a new decimal digit of the variable x. $h(p_{10},T)$ can be calculated using equations

$$h(p_{10},T) = \frac{10^n\{(1/10^n)\ell n\ (10^n)\}}{n} \qquad n \to \infty$$

$$= \ell n(10)$$

and a theorem of Kolmogorov[7] can be used to show that this is in fact the entropy of the transformation in this example, since the partition p_{10} is "generating" for this particular transformation.

$$h(T) = h(p_{10},T) = \ell n(10)$$

This can be associated with accuracy in a repeatability test by noting that in a test on this transformation one decimal digit of accuracy would be lost on each "turn".

We now apply these concepts to our transformation. Our "measure function" is the 4-D euclidian metric weighted by an exponential factor

$$e^{\frac{-(x^2+(\beta x')^2+(\beta y')^2+y^2)}{2\sigma^2}}$$

which simulates a gaussian beam. We have done repeatability tests with two "partitions": single precision and double precision.

For case B, trajectories picked randomly within this gaussian fall naturally into two groups:

1) 75% of the particles are "normal" with errors which grow as $(N)^{3/2}\ \delta$.

2) 25% are "chaotic" with errors which grow as $10^{aN}\ \delta$ with a $\simeq 10^{-3}$. There are very few ($\lesssim$1%) intermediate cases.

Normal trajectories, if as described above, have zero entropy and chaotic ones have a finite entropy. From the information above the entropy of the transformation can be estimated:

$$h(\delta,T) = .75 \cdot 0 + .25\ a$$

$$\cong 2.5 \times 10^{-4}$$

The same answer is obtained with single and double precision partitions, which provides empirical evidence that the number above is a supremum and

$$h(T) \cong 2.5 \times 10^{-4}$$

This entropy is significantly different from zero, and in fact quite large in view of the "non-chaotic" appearance of the transformation. (The reader is reminded that this estimate is not proved but is empirically derived from numerical evidence.)

"Stochastic trajectories" can obtain precise definition by requiring that these be trajectories which show "non-zero entropy". Our repeatability tests are evidence that these "chaotic" trajectories are cases of "stochastic motion".

IV. Entropy in Other Simulations

In case A and case C our repeatability tests[4,5,6] show no evidence of chaotic behavior in the trajectories tested. This indicates that "chaos" is limited to a "negligibly small" part of phase space at most, which in our simulations means ≤1%.

These cases had the same tune shift as case B but are in very different regions of tune space (ν_x, ν_y). Case A contains large 1/4 and other high order resonances, but has $\nu_x = \nu_y$ and has an additional kinematic

invariant from the equal tunes (as noted in reference 4) which may suppress the existence of chaotic behavior. Case C has $\nu_x \neq \nu_y$ but is free of resonances up to ninth order and therefore may not show as much chaotic behavior.

Our simulations give empirical evidence that the appearance of a significant amount of chaotic behavior at tune shifts that appear in $p\bar{p}$ collisions requires unequal tunes ($\nu_x \neq \nu_y$) and the appearance of low (<9th) order resonances in the tune spread. Further simulations and analyses can make these criteria more precise.

V. The Effect of Chaotic Trajectories

Longtime Beam Blow-Up

In references 4 and 5 we presented results of a 120 million turn simulation of Case B (equivalent to 40 minutes in the Tevatron), in which we search for long time beam blow-up due to the beam beam interaction. In Table 2 and Figures 6 A,B,C these results are duplicated, and these show RMS emittances of a 100-particle beam calculated as a function of time. The data points of Figures 6 A,B,C are the linearly extrapolated number of days needed to double the initial emittance, calculated from a linear fit to the simulation emittances from time t=0 to the data point time. (A negative number means emittance is decreasing.) Statistically significant changes are indicated by points inside the parabolic-like limit lines. There is evidence for a small exchange between x and y emittances ($\tilde{<}1\%$ in 20 minutes), but there is no change in the R-emittance, their rms sum.

As the present investigation determined, 21 of these trajectories are chaotic and have lost precise information of their initial positions after $\sim$100,000 turns. In order to investigate the role of chaotic trajectories in emittance changes, we generated a set of 100 trajectories, all of which are "normal". Results of a 60 million turn (20 minutes in Tevatron) simulation with this set are shown in Table 3 and Figures 7 A,B,C. No evidence for any change in emittances is seen, and in particular no exchange between x and y emittances.

This indicates that any changes seen in the previous simulation are due to chaotic trajectories. The smallness ($\sim$1%) of changes due to "chaotic" behavior possibly indicates that the major change in particle positions is in phase and not in amplitude. We speculate that this limitation in emittance changes is due to the "roundness" of the beam; a "flat" beam should be more phase sensitive. This speculation will be explored.

Also, since precise position information is lost in chaotic trajectories we are not able to determine whether the numerical emittance changes are physical or not. They may be artificially generated by the numerical errors. However, the smallness of the changes observed strongly suggests that any real changes in rms emittance introduced by "chaotic" trajectories in this case are small. The appearance of "chaotic" trajectories need not lead to beam blow-up.

We are grateful to Leo Michelotti for non-chaotic discussions on the meaning of chaos.

REFERENCES

1. Tevatron I Design Report, Fermilab, June 1980.
2. M. Month & J.C. Herrara, editors, Nonlinear Dynamics and the Beam-Beam Interaction, A.I.P. Conf. Proc. No. 57 (1979).
3. Proceedings of the Beam-Beam Interaction Seminar, SLAC, May 22-23, 1980, SLAC-PUB-2064.
4. D. Neuffer, A. Riddiford, A. Ruggiero, Fermilab Note FN-333, April 1981.
5. D. Neuffer, A. Riddiford, A. Ruggiero, Fermilab Note FN-343, 1981.
6. D. Neuffer, A. Riddiford, A. Ruggiero, IEEE Trans. on Nuclear Science NS-28, 1981.
7. Ya. G. Sinai, Introduction to Ergodic Theory, Princeton University Press, 1976.
8. Leo Michelotti, private discussions, 1981.

TABLE 1. Repeatability results for the 127 particles among the first 500 generated for Case B: $\nu_x = 0.245$, $\nu_y = 0.12$, $\Delta\nu = 0.01$. The particles were all run forward 100,000 turns (storing co-ordinates every 1250 turns) and back 100,000 turns. On the way back, the co-ordinates were subtracted from the forward co-ordinates and the error $\log_{10}\sqrt{(\Delta x)^2 + (\Delta y)^2 + (\beta_x \Delta x')^2 + (\beta_y \Delta y')^2}$ was compared with the cutoffs shown below. The first time the error crossed the cutoff, a linear interpolation estimated the turn number. That number was subtracted from 100,000 and the result doubled to find the numbers listed below.

Particle Number	Single Precision cutoff -9	cutoff -4	Double Precision cutoff -23	cutoff -18	cutoff -13	cutoff -8
1	11,846	26,254	10,840	53,704	68,592	85,868
2	3,804	32,596	2,736	13,322	25,964	35,354
8	1,984	11,950	486	18,472	63,710	74,188
9	5,474	14,126	6,544	11,774	16,054	23,716
14	5,010	13,358	6,274	14,928	22,924	28,826
19	2,726	15,040	3,504	20,270	33,746	49,854
21	13,478	23,820	9,816	26,174	38,546	52,834
30	10,432	29,128	6,164	28,984	40,594	58,374
33	6,486	14,558	3,540	10,806	15,252	21,934
34	7,668	17,758	8,782	18,382	30,152	45,750
35	4,530	17,126	3,996	21,988	41,474	61,530
36	2,920	16,644	3,892	9,724	25,046	46,010
37	10,524	25,998	9,322	18,196	25,080	34,258
44	5,016	21,448	3,508	10,326	16,562	43,248
54	11,416	21,086	8,706	18,588	35,594	43,048
55	6,254	11,156	4,084	12,228	30,738	40,482
61	3,852	11,732	3,060	8,770	14,846	27,050
75	8,144	24,026	5,654	12,576	26,316	34,476
77	4,408	15,100	10,784	48,000	80,644	97,998
94	17,804	157,742	12,416	149,226	(-17.43)	(-17.43)
96	3,898	23,246	6,004	22,370	50,236	80.874
102	7,454	18,520	8,428	17,054	27,904	37,912
103	5,288	18,078	3,470	12,918	30,596	40,630
111	20,668	34,984	8,616	29,408	38,886	44,754
122	2,586	19,412	5,058	17,682	24,194	30,510
124	5,704	14,192	6,250	14,902	27,592	37,890
125	7,232	29,896	7,438	39,758	63,750	97,906

continued

TABLE 1 continued (Case B)

Particle Number	Single Precision cutoff -9	Single Precision cutoff -4	Double Precision cutoff -23	Double Precision cutoff -18	Double Precision cutoff -13	Double Precision cutoff -8
128	11,814	67,018	5,262	20,310	33,538	51,504
129	10,430	140,336	8,410	139,078	(-15.09)	(-15.09)
132	9,168	18,424	4,248	15,964	32,416	39,868
135	3,688	10,358	4,226	14,690	28,704	37,032
141	<1,250	13,538	7,258	171,434	188,772	199,198
143	4,492	12,924	5,846	17,476	30,378	46,938
144	5,990	34,816	4,596	19,688	43,186	61,802
148	4,774	17,802	6,250	36,244	68,748	82,884
154	3,300	11,210	7,156	14,002	30,348	39,108
155	5,286	15,676	5,442	14,648	23,568	31,216
160	8,092	25,138	23,956	63,990	86,414	100,264
164	9,330	19,534	5,672	15,120	25,924	33,678
167	3,066	12,038	4,080	23,766	28,986	35,596
168	5,258	13,242	4,028	10,076	16,216	22,108
171	7,292	23,634	6,330	16,440	28,416	38,304
174	16,380	49,186	4,510	16,500	25,602	34,314
179	5,822	13,580	8,244	24,564	31,028	39,226
187	3,364	12,398	5,914	16,506	21,992	27,756
192	3,068	10,320	6,710	15,474	21,392	28,980
194	7,294	17,668	11,556	31,778	47,982	54,828
199	6,440	17,516	5,178	24,678	29,612	44,190
203	7,344	14,380	17,524	33,582	42,494	52,900
209	6,096	12,456	5,998	21,808	33,374	44,326
215	3,570	11,592	2,750	15,044	19,886	30,092
218	7,460	22,966	18,472	27,246	48,826	60,598
219	4,724	15,416	7,192	21,404	40,298	51,288
221	6,988	18,478	4,494	12,002	20,244	28,476
224	9,934	36,090	4,852	17,376	30,576	40,944
225	6,342	19,130	7,588	18,974	28,878	38,636
234	3,576	23,246	5,294	20,788	36,256	49,878
238	24,380	48,274	17,830	46,246	55,140	67,070
244	8,656	23,428	11,368	22,654	38,036	53,456
247	5,700	17,176	3,504	8,526	13,352	20,096
250	3,672	13,610	<1,250	16,674	28,480	40,972

continued

TABLE 1 continued (Case B)

Particle Number	Single Precision cutoff -9	Single Precision cutoff -4	Double Precision cutoff -23	Double Precision cutoff -18	Double Precision cutoff -13	Double Precision cutoff -8
254	3,708	10,234	5,066	14,156	22,498	32,502
255	4,818	10,698	9,430	25,138	33,074	39,782
256	5,912	15,260	4,152	11,714	16,678	27,920
260	7,902	13,708	6,826	14,860	26,578	34,864
261	7,164	18,974	3,642	18,078	31,996	44,276
266	7,228	16,174	5,172	14,628	27,026	39,106
267	3,238	20,538	7,094	25,688	39,860	58,286
269	5,492	47,110	8,822	24,710	99,998	164,796
271	12,364	29,040	6,620	15,376	24,094	33,970
278	4,958	14,772	5,216	14,434	34,578	40,800
284	5,494	18,512	9,632	24,374	31,322	39,042
288	11,680	23,216	8,982	16,984	29,960	39,418
292	11,184	19,468	6,578	16,770	29,156	42,310
294	15,020	83,042	5,682	16,416	30,434	43,912
297	14,702	28,024	4,802	29,616	56,726	76,374
301	7,256	62,664	16,356	89,282	127,912	155,494
302	25,640	131,060	19,070	131,240	(-13.34)	(-13.34)
303	3,884	11,138	5,020	14,262	27,604	33,668
305	3,802	12,508	3,716	10,698	18,492	22,624
307	5,606	13,288	3,810	13,332	19,100	24,722
314	5,228	16,814	2,930	10,196	24,420	34,826
320	18,460	42,722	13,164	30,022	52,176	70,158
323	6,454	32,930	6,690	17,034	43,220	85,800
329	6,048	13,674	5,348	20,314	38,276	46,590
331	6,256	18,192	5,608	41,636	58,406	97,684
337	13,170	122,134	7,306	35,870	82,532	100,364
339	16,894	50,164	10,512	28,228	39,728	53,258
347	6,182	11,372	4,704	15,322	24,244	33,036
348	4,688	12,090	7,074	15,224	28,524	34,914
357	3,550	8,756	3,132	10,274	16,814	26,410
359	5,242	10,990	9,494	17,928	26,650	34,992
360	7,550	22,002	6,910	47,110	71,114	84,714
364	6,274	16,992	3,766	17,052	28,610	46,302
366	17,510	35,680	7,188	49,808	70,386	84,650

continued

TABLE 1 continued (Case B)

Particle Number	Single Precision cutoff -9	Single Precision cutoff -4	Double Precision cutoff -23	Double Precision cutoff -18	Double Precision cutoff -13	Double Precision cutoff -8
368	6,030	15,206	4,868	9,150	19,474	25,378
370	3,696	11,282	5,586	10,930	19,332	26,154
373	45,860	80,468	17,766	33,998	50,812	64,890
381	25,726	40,830	7,174	24,886	36,262	50,538
383	5,950	15,896	7,892	19,220	30,048	36,428
392	4,890	13,786	13,586	26,162	42,130	59,044
398	6,794	17,142	5,244	12,988	19,868	28,728
406	7,834	16,338	13,738	36,006	51,822	61,174
418	22,754	63,382	13,326	40,916	62,200	107,678
421	4,248	10,542	3,792	15,966	25,648	30,626
422	5,674	19,280	10,006	20,010	29,638	36,734
423	3,936	9,446	5,762	18,150	25,476	46,156
424	4,406	14,744	5,168	14,626	22,926	30,196
425	4,038	19,650	3,650	33,954	80,190	92,372
431	23,014	39,310	11,486	23,792	34,370	49,272
441	7,250	19,296	9,662	20,186	33,566	40,780
442	4,642	10,578	3,502	17,082	28,518	35,618
445	3,656	9,720	4,736	25,702	46,562	62,984
447	4,500	15,698	7,110	24,964	50,818	59,394
452	3,976	14,942	4,518	10,962	19,082	25,380
462	3,956	11,292	5,780	16,602	30,248	35,726
464	7,734	14,190	5,480	10,362	20,312	30,438
465	5,886	17,114	5,366	19,718	25,240	36,246
466	4,126	13,708	5,170	27,120	45,718	62,958
470	8,060	43,588	4,970	30,808	64,142	146,862
480	7,738	20,246	5,268	11,770	19,692	30,170
481	6,116	13,650	8,132	20,460	27,254	42,690
482	9,490	47,866	9,516	42,502	63,862	71,200
485	6,074	12,164	3,876	12,342	23,742	28,152
486	5,996	11,840	4,832	22,716	32,366	43,126
487	4,660	16,794	3,124	10,900	17,460	24,404
489	4,582	28,166	6,088	17,516	23,600	34,402

CONCLUDED

TABLE 2. Emittance data for Case B. $\nu_x = 0.245$; $\nu_y = 0.120$; $\Delta\nu = 0.010$
Cumulative values.

Real Ring Time (min)	Million Turns	X_{av}	Doubling Time (days)	Y_{av}	Doubling Time (days)	R_{av}	Doubling Time (days)
$\frac{2}{3}$	2	0.0227520	0.2	0.0192872	0.1	0.0298409	0.1
$1\frac{1}{3}$	4	0.0227605	0.7	0.0193705	0.1	0.0299023	0.1
2	6	0.0227589	1.5	0.0193918	0.1	0.0299149	0.3
$2\frac{2}{3}$	8	0.0227293	-0.3	0.0193824	0.6	0.0298863	-0.8
$3\frac{1}{3}$	10	0.0227243	-0.4	0.0193464	-0.3	0.0298592	-0.4
4	12	0.0227275	-1.3	0.0193089	-0.2	0.0298374	-0.4
$4\frac{2}{3}$	14	0.0227243	2.0	0.0193784	-0.2	0.0298298	-0.5
$5\frac{1}{3}$	16	0.0227431	2.8	0.0192687	-0.2	0.0298235	-0.6
6	18	0.0227731	0.5	0.0192616	-0.3	0.0298419	-2.5
$6\frac{2}{3}$	20	0.0227619	1.1	0.0192598	-0.4	0.0298323	-1.5
$7\frac{1}{3}$	22	0.0227764	0.8	0.0192621	-0.5	0.0298447	37.
8	24	0.0227892	0.6	0.0192630	-0.7	0.0298550	3.1
$8\frac{2}{3}$	26	0.0228057	0.5	0.0192650	-1.0	0.0298687	1.5
$9\frac{1}{3}$	28	0.0228304	0.4	0.0192609	-1.0	0.0298850	1.0
10	30	0.0228423	0.4	0.0192612	-1.3	0.0298944	0.9
$10\frac{2}{3}$	32	0.0228507	0.4	0.0192610	-1.5	0.0299007	1.0
$11\frac{1}{3}$	34	0.0228483	0.5	0.0192603	-1.7	0.0298985	1.3
12	36	0.0228320	1.0	0.0192638	-2.6	0.0298883	2.2
$12\frac{2}{3}$	38	0.0228238	1.5	0.0192628	-2.8	0.0298814	4.2
$13\frac{1}{3}$	40	0.0228216	1.9	0.0192602	-2.6	0.0298782	7.2
14	42	0.0228252	1.9	0.0192582	-2.5	0.0298796	6.9
$14\frac{2}{3}$	44	0.0228277	1.9	0.0192593	-3.2	0.0298822	5.7
$15\frac{1}{3}$	46	0.0228280	2.2	0.0192599	-3.9	0.0298828	6.0
16	48	0.0228312	2.1	0.0192581	-3.6	0.0298841	6.0
$16\frac{2}{3}$	50	0.0228347	1.9	0.0192597	-4.9	0.0298878	4.8
$17\frac{1}{3}$	52	0.0228339	2.4	0.0192654	-26.	0.0298908	4.2
18	54	0.0228401	1.9	0.0192605	-6.7	0.0298924	4.2
$18\frac{2}{3}$	56	0.0228499	1.5	0.0192590	-5.9	0.0298990	3.3
$19\frac{1}{3}$	58	0.0228554	1.5	0.0192570	-5.1	0.0299019	3.1
20	60	0.0228630	1.3	0.0192567	-5.4	0.0299076	2.7

TABLE 2

TABLE 2 (continued)

Real Ring Time (min)	Million Turns	X_{av}	Doubling Time (days)	Y_{av}	Doubling Time (days)	R_{av}	Doubling Time (days)
$20\frac{2}{3}$	62	0.0228672	1.3	0.0192580	-7.2	0.0299115	2.6
$21\frac{1}{3}$	64	0.0228724	1.3	0.0192597	-11.0	0.0299167	2.4
22	66	0.0228687	1.5	0.0192553	-5.8	0.0299110	3.2
$22\frac{2}{3}$	68	0.0228658	1.8	0.0192529	-5.0	0.0299072	4.2
$23\frac{1}{3}$	70	0.0228660	2.0	0.0192506	-4.4	0.0299058	5.0
24	72	0.0228666	2.1	0.0192479	-3.9	0.0299045	5.9
$24\frac{2}{3}$	74	0.0228645	2.5	0.0192450	-3.5	0.0299011	8.6
$25\frac{1}{3}$	76	0.0228599	3.3	0.0192422	-3.2	0.0298957	21.1
26	78	0.0228599	3.5	0.0192396	-3.0	0.0298940	38.2
$26\frac{2}{3}$	80	0.0228646	3.1	0.0192380	-3.0	0.0298966	19.5
$27\frac{1}{3}$	82	0.0228682	2.8	0.0192374	-3.1	0.0298989	13.9
28	84	0.0228650	3.5	0.0192350	-3.0	0.0298950	36.3
$28\frac{2}{3}$	86	0.0228694	3.1	0.0192336	-3.0	0.0298974	20.3
$29\frac{1}{3}$	88	0.0228664	3.8	0.0192321	-3.0	0.0298942	68.8
30	90	0.0228648	4.4	0.0192288	-2.8	0.0298908	-55.6
$30\frac{2}{3}$	92	0.0228633	5.1	0.0192278	-2.8	0.0298890	-30.0
$31\frac{1}{3}$	94	0.0228636	5.3	0.0192293	-3.2	0.0298902	-50.3
32	96	0.0228650	5.2	0.0192317	-3.9	0.0298929	216.
$32\frac{2}{3}$	98	0.0228660	5.2	0.0192327	-4.4	0.0298942	61.8
$33\frac{1}{3}$	100	0.0228656	5.7	0.0192341	-5.0	0.0298948	50.1
34	102	0.0228661	5.9	0.0192342	-5.4	0.0298952	44.2
$34\frac{2}{3}$	104	0.0228686	5.3	0.0192352	-6.2	0.0298978	23.5
$35\frac{1}{3}$	106	0.0228703	5.1	0.0192357	-6.8	0.0298995	18.9
36	108	0.0228711	5.2	0.0192379	-8.9	0.0299014	15.2
$36\frac{2}{3}$	110	0.0228697	5.9	0.0192391	-10.9	0.0299011	16.8
$37\frac{1}{3}$	112	0.0228706	5.9	0.0192429	-24.0	0.0299043	12.4
38	114	0.0228705	6.3	0.0192445	-46.9	0.0299052	12.0
$38\frac{2}{3}$	116	0.0228687	7.5	0.0192463	+985.	0.0299050	12.9
$39\frac{1}{3}$	118	0.0228668	9.2	0.0192462	-801.	0.0299034	16.0
40	120	0.0228629	14.7	0.0192472	+93.5	0.0299012	23.0

TABLE 3. Emittance data for Case B: $\nu_x = 0.245$, $\nu_y = 0.120$, $\Delta\nu = 0.010$
Cumulative values; 21 new particles.

Real Ring Time (min)	Million turns	X_{av} (mm-mrad)	Doubling Time (days)	Y_{av} (mm-mrad)	Doubling Time (days)	R_{av} (mm-mrad)	Doubling Time (days)
$\frac{2}{3}$	2	0.0214431	0.250	0.0153091	0.137	0.0263579	0.203
$1\frac{1}{3}$	4	0.0214426	-47.3	0.0153007	-1.73	0.0263528	-4.73
2	6	0.0214540	0.584	0.0153019	-26.0	0.0263628	0.890
$2\frac{2}{3}$	8	0.0214524	2.00	0.0153008	-10.7	0.0263615	3.26
$3\frac{1}{3}$	10	0.0214596	1.02	0.0153030	4.96	0.0263681	1.38
4	12	0.0214559	3.61	0.0153003	-4.99	0.0263635	8.20
$4\frac{2}{3}$	14	0.0214562	4.79	0.0153014	-30.9	0.0263644	7.58
$5\frac{1}{3}$	16	0.0214496	-3.35	0.0152990	-4.30	0.0263576	-3.66
6	18	0.0214495	-4.54	0.0152976	-3.57	0.0263568	-4.24
$6\frac{2}{3}$	20	0.0214466	-3.15	0.0152950	-2.46	0.0263529	-2.90
$7\frac{1}{3}$	22	0.0214491	-8.51	0.0152964	-4.61	0.0263557	-6.63
8	24	0.0214489	-10.2	0.0152957	-4.88	0.0263552	-7.49
$8\frac{2}{3}$	26	0.0214513	46.4	0.0152961	-7.30	0.0263573	-31.0
$9\frac{1}{3}$	28	0.0214513	60.5	0.0152958	-7.84	0.0263571	-31.9
10	30	0.0214515	49.7	0.0152968	-21.4	0.0263580	-1410.
$10\frac{2}{3}$	32	0.0214504	-47.1	0.0152969	-29.0	0.0263571	-42.1
$11\frac{1}{3}$	34	0.0214486	-13.1	0.0152973	-85.3	0.0263559	-18.9
12	36	0.0214489	-17.9	0.0152975	1200.	0.0263562	-28.3
$12\frac{2}{3}$	38	0.0214478	-12.6	0.0152977	110.	0.0263555	-20.6
$13\frac{1}{3}$	40	0.0214491	-33.3	0.0152980	51.4	0.0263567	-83.9
14	42	0.0214485	-22.4	0.0152982	43.2	0.0263563	-49.0
$14\frac{2}{3}$	44	0.0214507	49.0	0.0152989	21.1	0.0263586	32.7
$15\frac{1}{3}$	46	0.0214497	-138.	0.0152985	39.7	0.0263575	242.
16	48	0.0214509	44.4	0.0152993	19.2	0.0263589	31.0
$16\frac{2}{3}$	50	0.0214490	-41.7	0.0152986	43.5	0.0263570	-126.
$17\frac{1}{3}$	52	0.0214495	-86.5	0.0152995	21.1	0.0263578	123.
18	54	0.0214477	-20.7	0.0152992	29.9	0.0162562	-48.2
$18\frac{2}{3}$	56	0.0214487	-45.3	0.0152996	24.2	0.0263573	-1310.
$19\frac{1}{3}$	58	0.0214484	-38.9	0.0152986	120.	0.0263564	-69.1
20	60	0.0214494	-225.	0.0152988	71.2	0.0263574	714.

Figure 1. Repeatability errors; Case B: $\nu_x = 0.245$; $\nu_y = 0.120$; $\Delta\nu = 0.010$
Initial Conditions: $X'_o = Y'_o = 0$
$X_o = Y_o = A\sigma$, where A = 0.5, 1.0 and 2.0; $\sigma = 0.08165$ mm

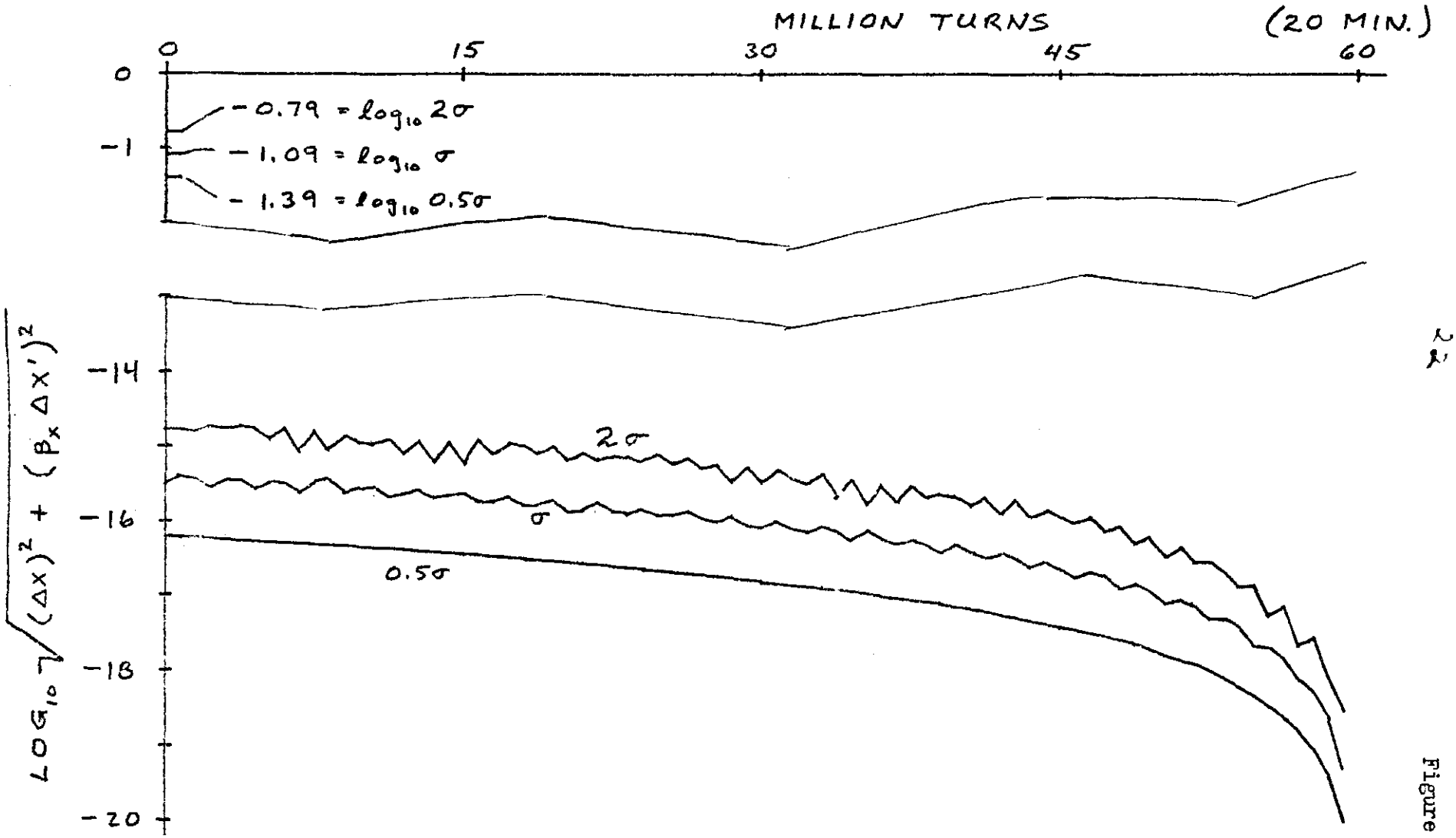

Figure 1

Figure 2. Repeatability errors; Case B: $\nu_x = 0.245$; $\nu_y = 0.120$; $\Delta\nu = 0.010$
Initial Conditions: $X_o = Y_o = 1.5\sigma = 0.1225$ mm; $X'_o = Y'_o = 0$

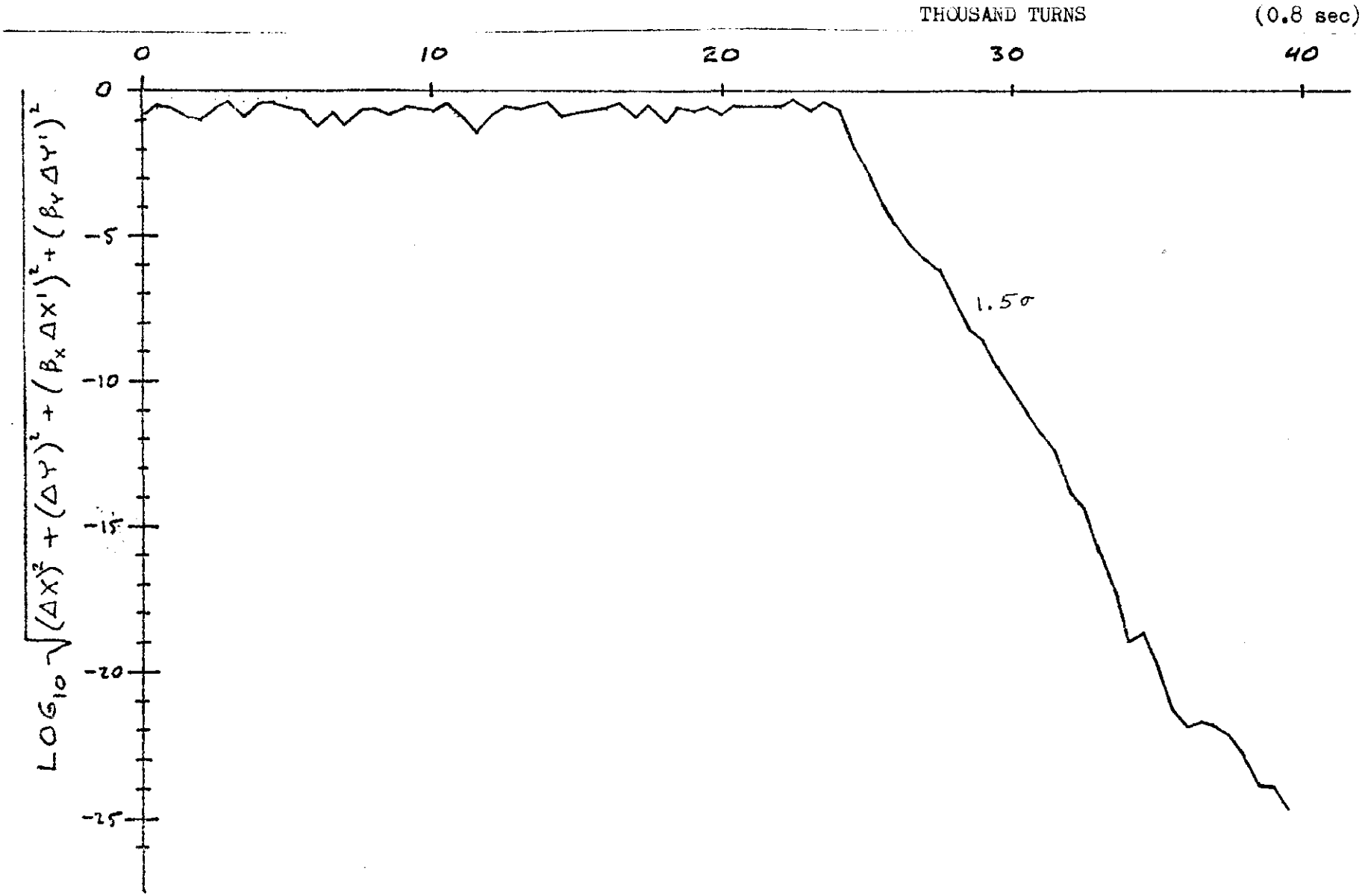

Figure 2

Figure 3. Comparison (single precision vs. double precision) of the number of turns required for the error to reach the cutoff value -2, for the 20 particles that fail in the first 100 generated for Case B: $\nu_x = 0.245$; $\nu_y = 0.120$; $\Delta\nu = 0.010$. The single precision results show a loss of about 12 decimals of accuracy while the double precision results show a loss of about 26 decimals of accuracy.

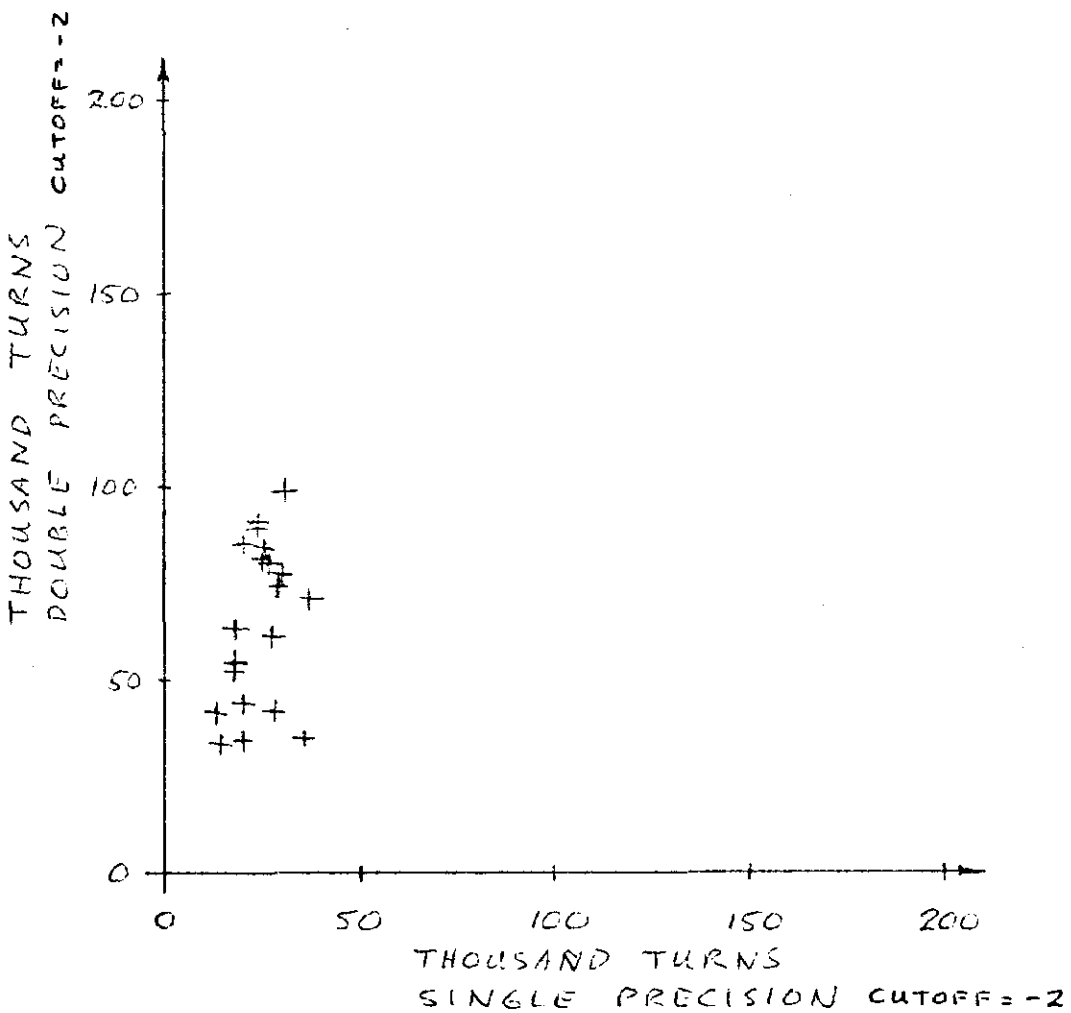

Figure 4A Initial coordinates of the 100 particles used in Case B: $\nu_x = 0.245$; $\nu_y = 0.120$; $\Delta\nu = 0.010$
The 21 circled particles lose all accuracy in a few hundred thousand turns.

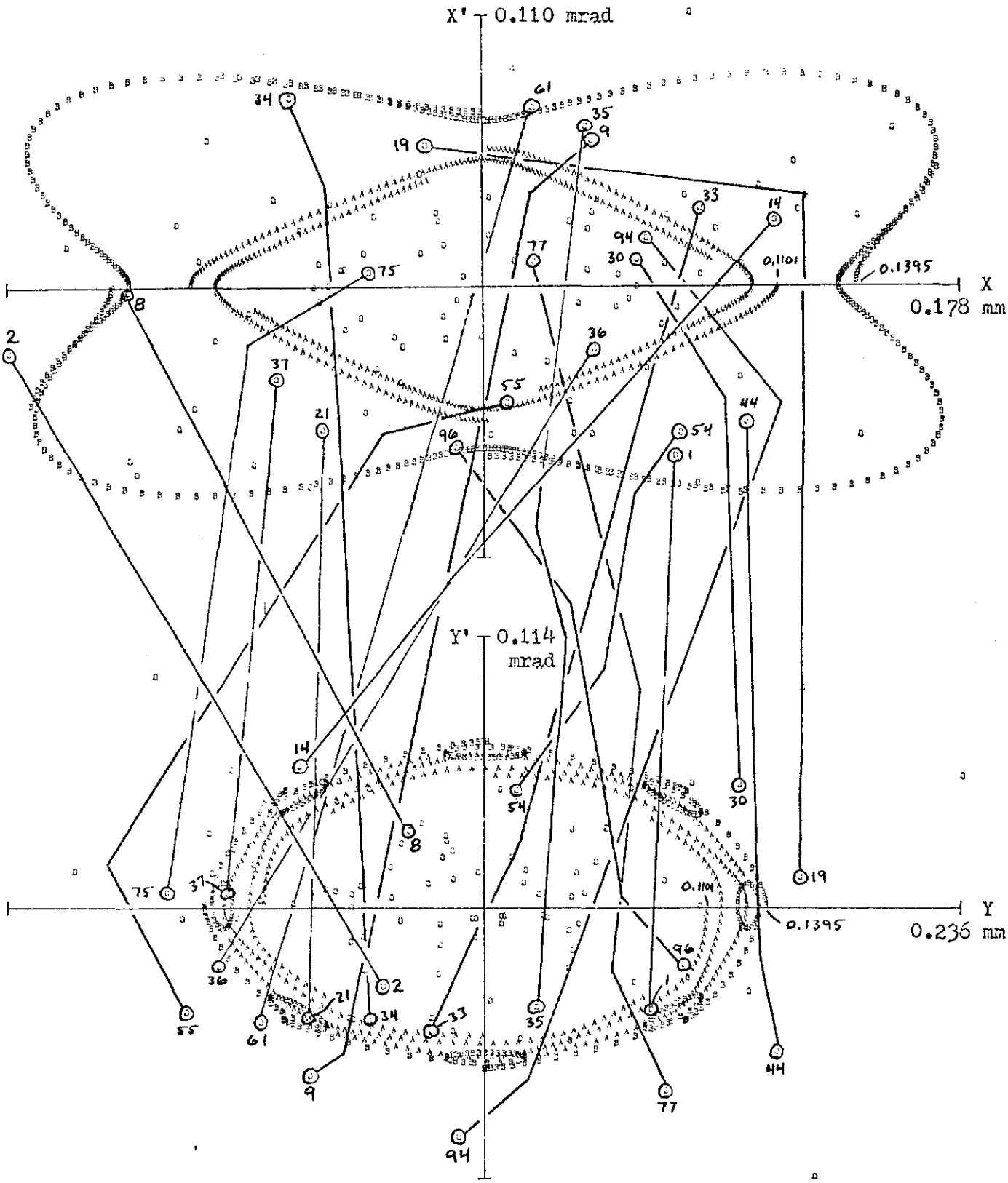

Figure 4B. (X,X') and (Y,Y') phase plane plots of the 127 particle initial values out of 500 which lose accuracy by about 200,000 turns. Case B: $\nu_x = 0.245$; $\nu_y = 0.120$; $\Delta\nu = 0.010$

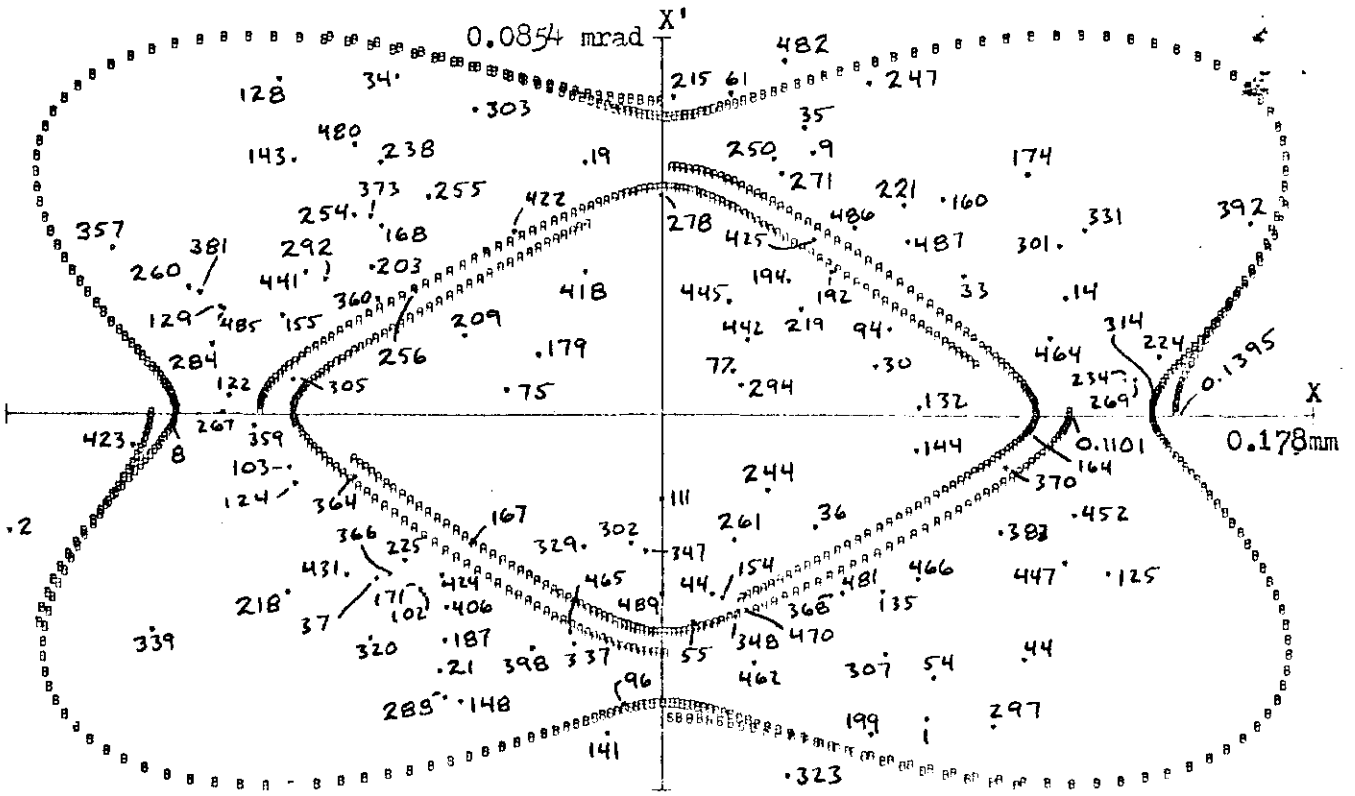

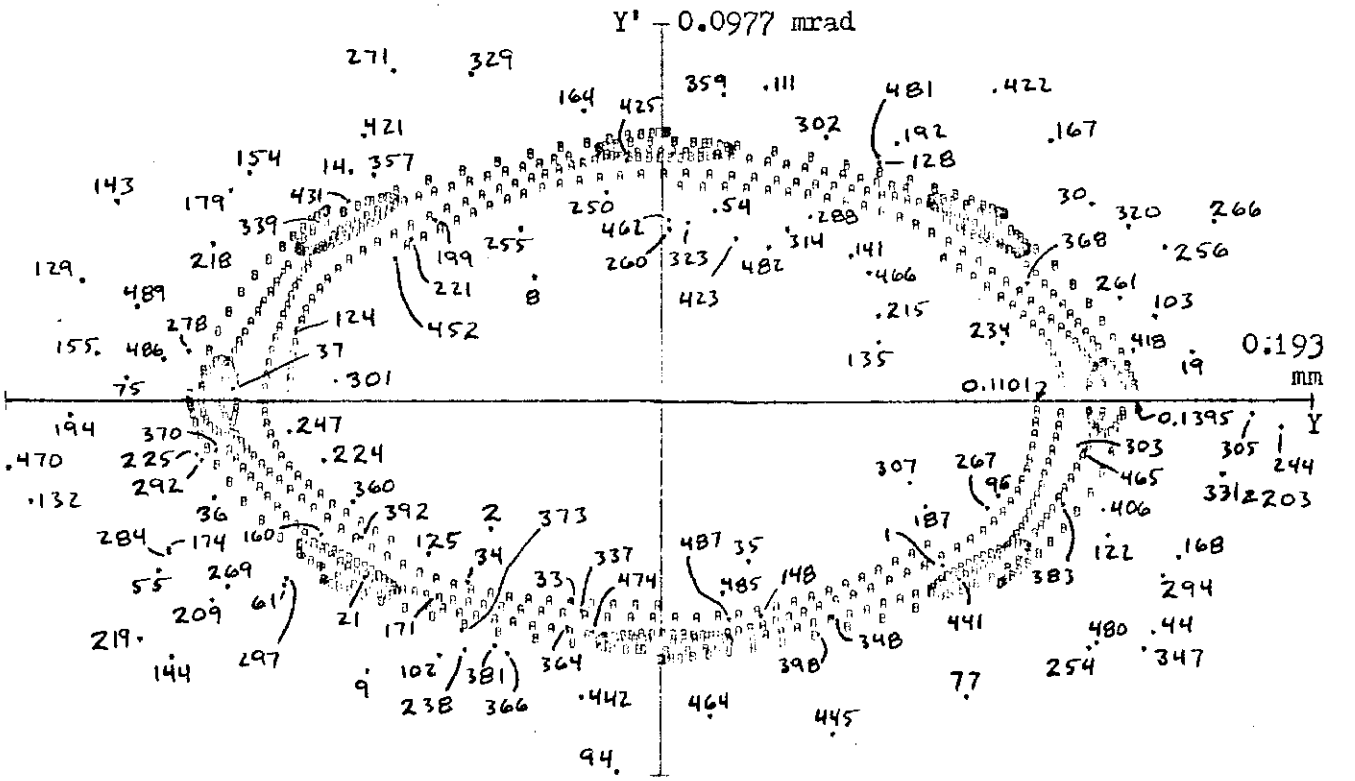

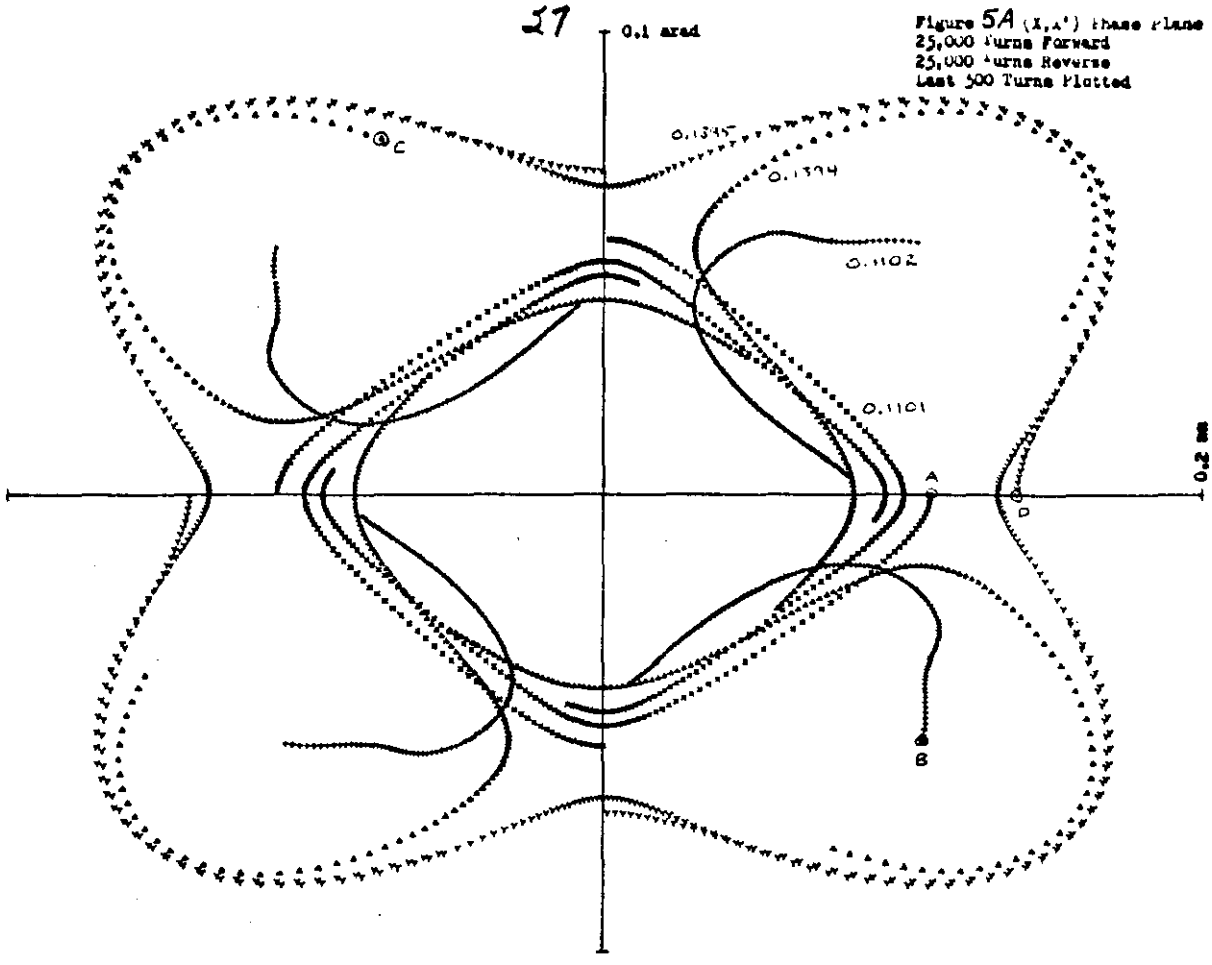

Figure 5A (X,X') Phase Plane
25,000 Turns Forward
25,000 Turns Reverse
Last 500 Turns Plotted

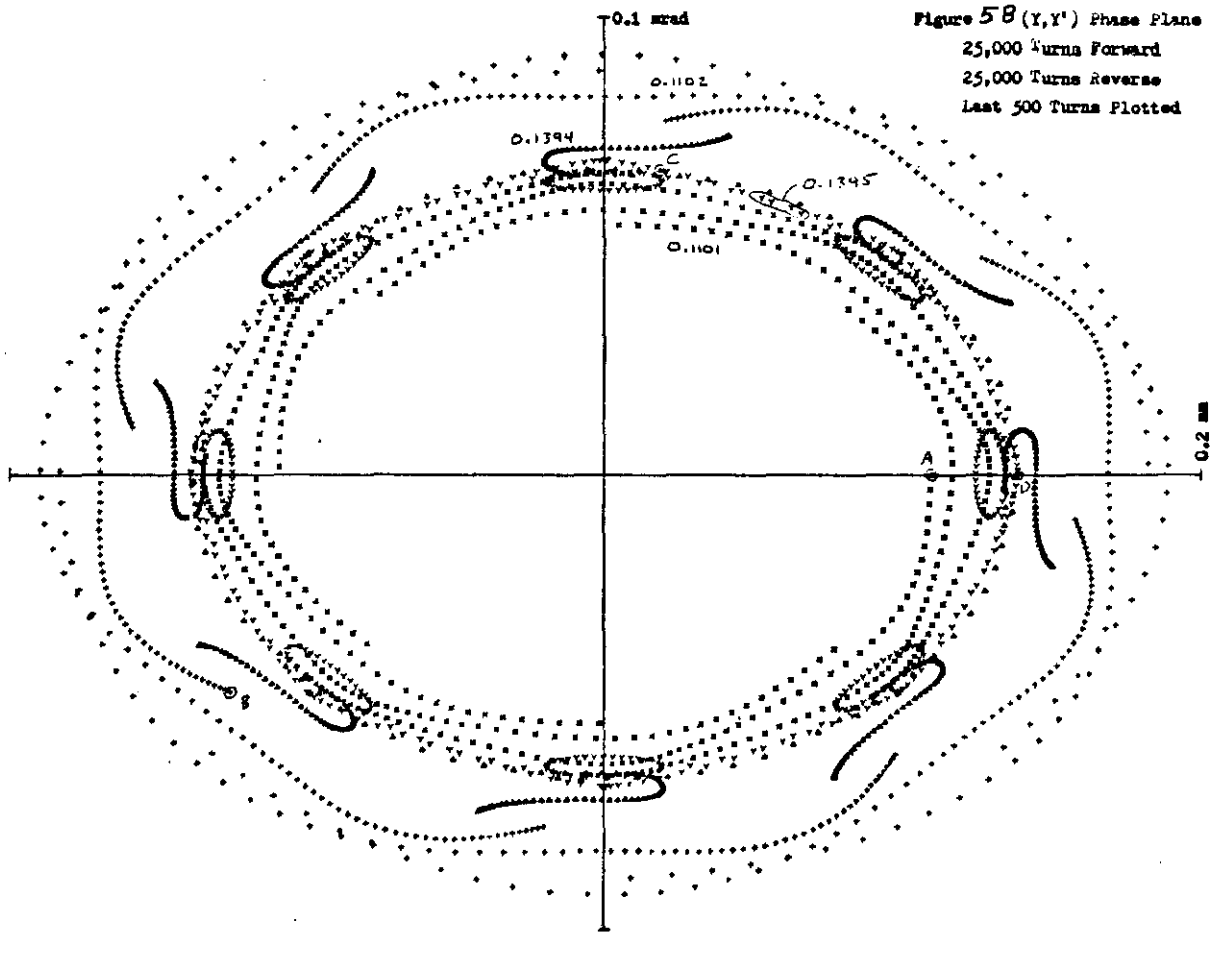

Figure 5B (Y,Y') Phase Plane
25,000 Turns Forward
25,000 Turns Reverse
Last 500 Turns Plotted

Figure 6. Comparison of cumulative doubling times with statistically significant doubling times.
Case B: $\nu_x = 0.245$; $\nu_y = 0.120$; $\Delta\nu = 0.010$

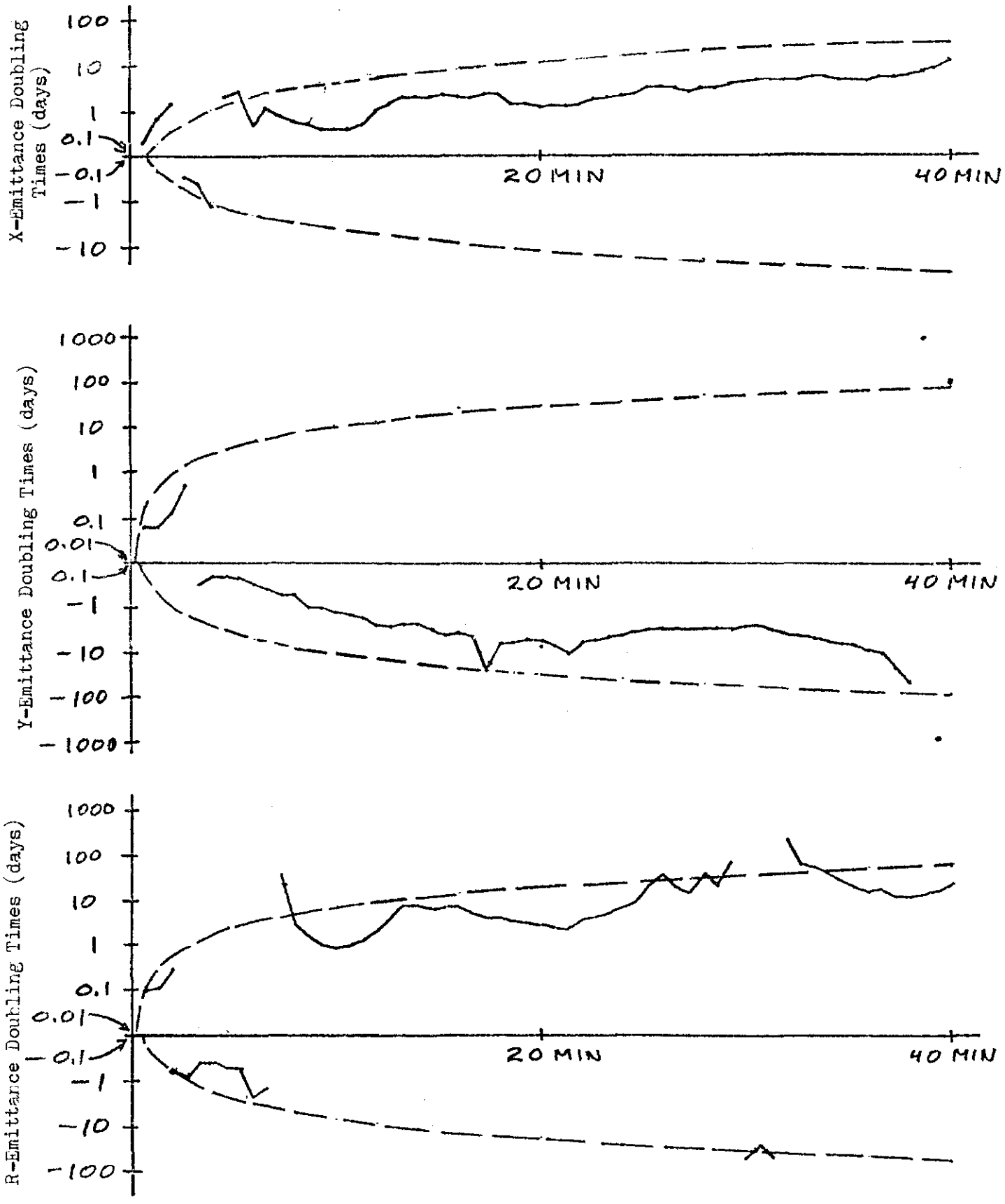

Figure 7A. Comparison of X-emittance cumulative doubling times with statistically significant doubling times.
Case B: $\nu_x = 0.245$, $\nu_y = 0.120$, $\Delta\nu = 0.010$
21 new particles

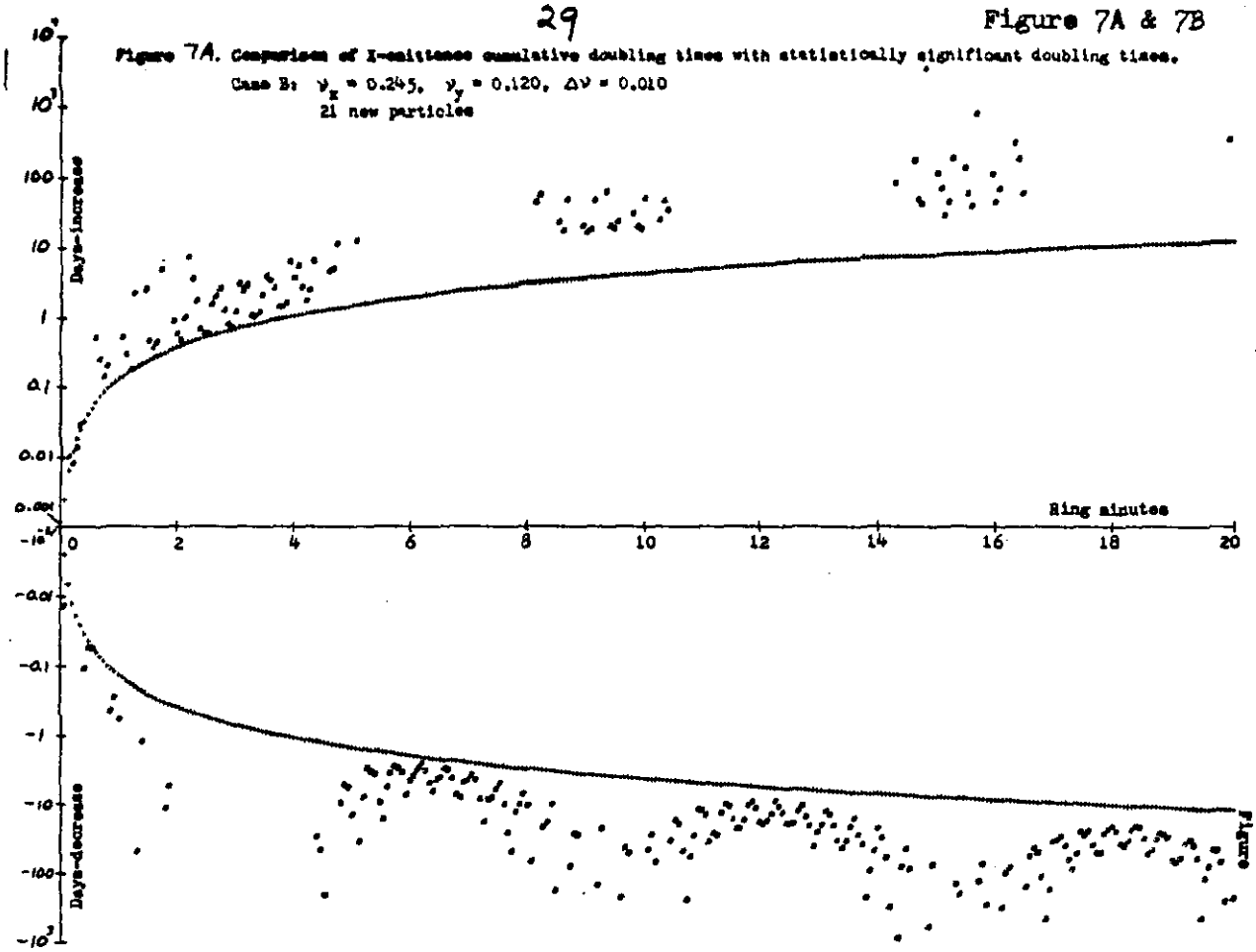

Figure 7B. Comparison of Y-emittance cumulative doubling times with statistically significant doubling times.
Case B: $\nu_x = 0.245$, $\nu_y = 0.120$, $\Delta\nu = 0.010$
21 new particles

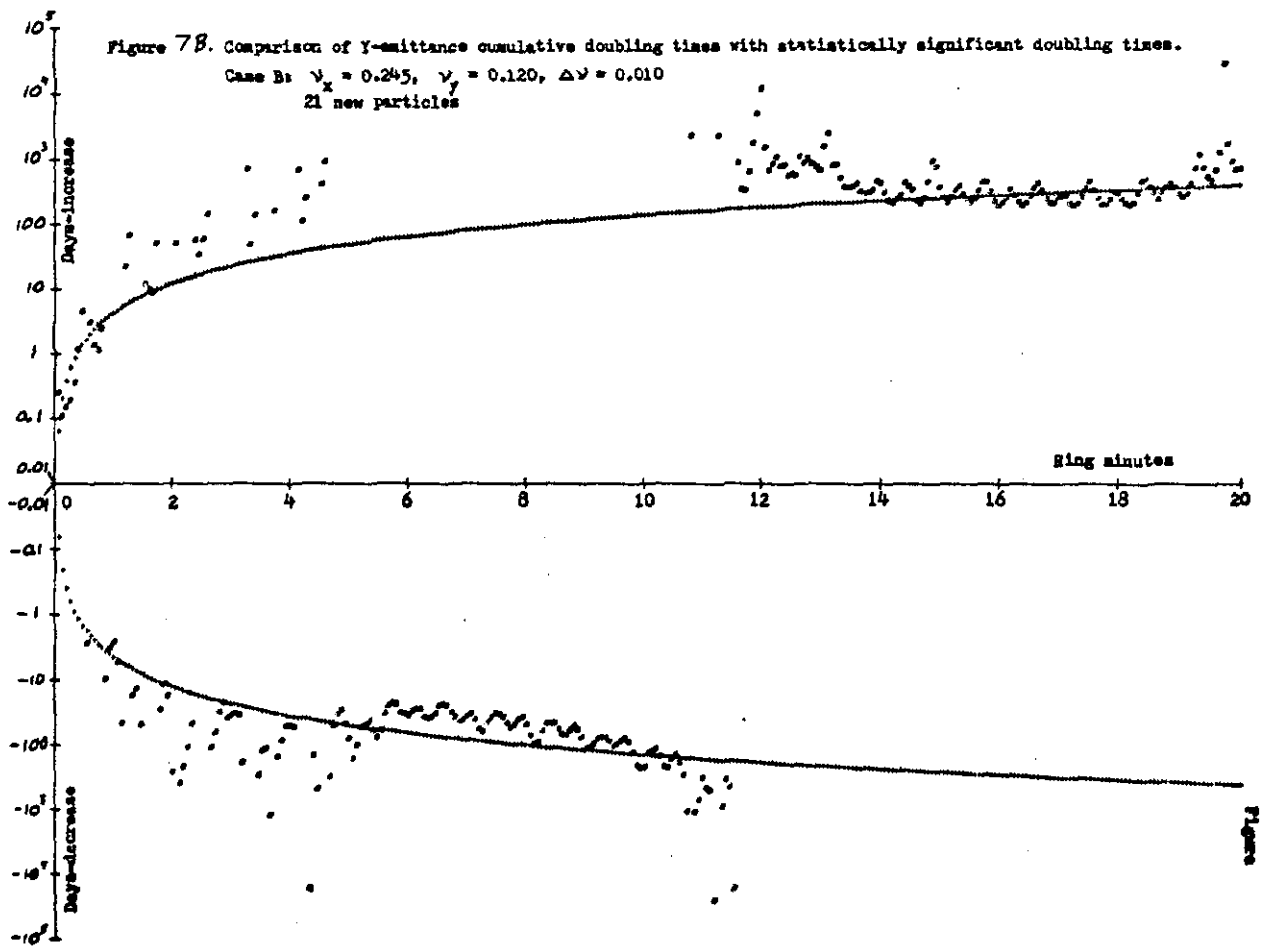

Figure 7C. Comparison of R-emittance cumulative doubling times with statistically significant doubling times.
Case B: $\nu_x = 0.245$, $\nu_y = 0.120$, $\Delta\nu = 0.010$
21 new particles

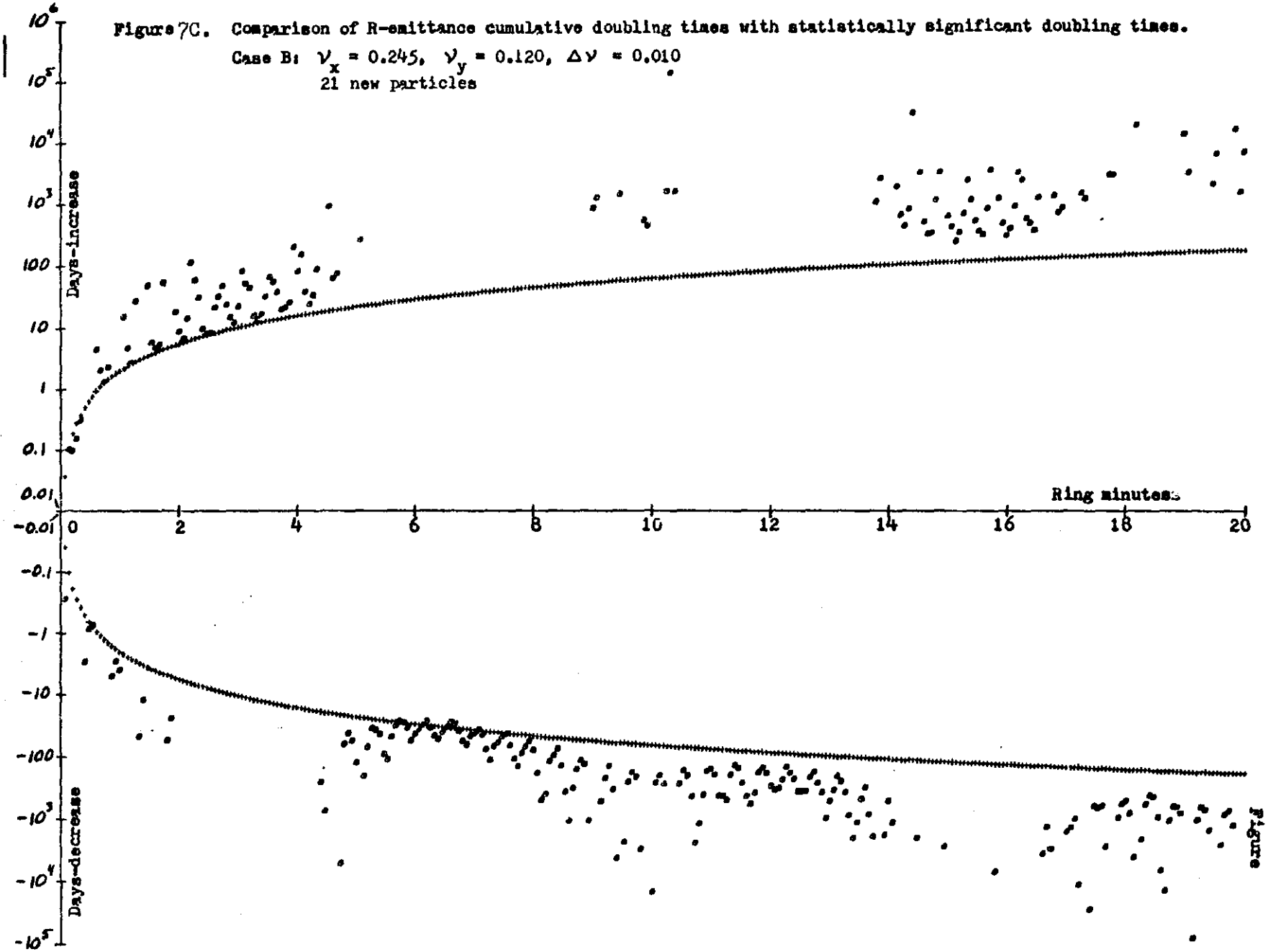

Figure 7C